JGR Atmospheres

RESEARCH ARTICLE
10.1029/2022JD037980

Key Points:

- Canopy density is the first-order control on increases in longwave radiation to snow beneath forests away from canopy gaps and edges
- Sub-canopy air temperature is an effective proxy for canopy temperature in calculating downward emission of longwave radiation
- Above-canopy air temperature is a less effective proxy, but a canopy model driven with above-canopy temperature has lower errors

Correspondence to:
N. Rutter,
nick.rutter@northumbria.ac.uk

Citation:
Rutter, N., Essery, R., Baxter, R., Hancock, S., Horton, M., Huntley, B., et al. (2023). Canopy structure and air temperature inversions impact simulation of sub-canopy longwave radiation in snow-covered boreal forests. *Journal of Geophysical Research: Atmospheres*, *128*, e2022JD037980. https://doi.org/10.1029/2022JD037980

Received 9 OCT 2022
Accepted 6 JUL 2023

Canopy Structure and Air Temperature Inversions Impact Simulation of Sub-Canopy Longwave Radiation in Snow-Covered Boreal Forests

Nick Rutter[1], Richard Essery[2], Robert Baxter[3], Steven Hancock[2,3], Maya Horton[1], Brian Huntley[3], Tim Reid[2], and John Woodward[1]

[1]Department of Geography and Environmental Sciences, Northumbria University, Newcastle upon Tyne, UK, [2]School of GeoSciences, University of Edinburgh, Edinburgh, UK, [3]Department of Biosciences, Durham University, Durham, UK

Abstract Longwave radiation is often the dominant source of energy for snowmelt in forests. Measurements at forest sites of varying density in Sweden and Finland show that downwelling longwave radiation is enhanced under forest canopies, even for sparse canopies and particularly for clear skies. Canopy density must be estimated accurately to predict this enhancement. Linear regression with above-canopy longwave radiation and air temperature as predictors of sub-canopy radiation gives good predictions of sub-canopy longwave radiation with weightings for transmission through canopy gaps that are close to measured sky view fractions. Air temperature serves here as a proxy for effective canopy radiative temperature. Adding above-canopy shortwave radiation as a predictor gives little improvement in the predictions, suggesting that daytime heating of trunks above the air temperature ("hot trees") has limited influence on longwave radiation under these continuous canopies. The influence of canopy temperatures falling below the above-canopy air temperature ("cold trees") on calm, clear nights, however, is apparent. Decoupling of canopy and above-canopy air temperatures in an energy balance model of the type used in large-scale land surface modeling allows this cooling.

Plain Language Summary Longwave radiation is a component of the total energy budget between the atmosphere and the land surface. It is often the most important source of energy for snowmelt in forests. The amount of longwave radiation received by snow depends on the temperature and thermal emissivity of the forest canopy and sky. Forest canopies usually have higher emissivities than the sky and forests enhance longwave radiation, so accurate estimation of forest canopy density is critical for simulation of longwave radiation to the snow surface. Air temperature works well as a proxy for forest canopy temperature in boreal forests in Sweden and Finland. However, whether the air temperature used as a proxy is measured above or below a forest canopy can be important. Usually, above canopy air temperature works well as a proxy, but on calm, clear nights, forest canopy temperatures fall much lower than above canopy air temperatures. These periods of low canopy temperature require decoupling from above canopy air temperature by a model to simulate longwave radiation more accurately to snow.

1. Introduction

Boreal forests strongly mediate winter and spring energy fluxes between the atmosphere and the snow-covered land surface. The overlapping area of snow and boreal forest annually covers up to ~8.9 million km^2 of the Northern Hemisphere (Rutter et al., 2009). Forest canopy structure varies widely across boreal forests, ranging from sparse canopies in forest-shrub and forest-grassland ecotones at altitudinal and latitudinal tree lines, to forest gaps in discontinuous canopy cover, through to continuous canopy cover in dense boreal forest. With increasing canopy cover, energy fluxes at the snow-covered land surface become increasingly dominated by longwave emittance, which is largely controlled by the temperature of canopy elements (trunks, branches, needles) facing the snow surface. Where canopy radiative temperatures are greater than those of the snow surface, especially during melt periods when maximum snow surface temperatures are limited to 0°C, positive net longwave fluxes into snow dominate the energy balance (Hotovy & Jenicek, 2020; Webster et al., 2016), increasing melt rates (Lundquist et al., 2013) and land surface warming. When canopy temperatures are cooler than the snow surface, negative net longwave fluxes may delay surface warming. Hence, longwave radiation to sub-canopy snow in

boreal forests has considerable implications for the timing of water availability, ecological functioning, and forest micrometeorology.

Simulation of sub-canopy longwave radiation requires accurate parameterization of forest canopy temperature to combine the usually cooler downwelling atmospheric component of total longwave radiation with that of the warmer forest canopy. Such two-component partitioning allows effective model parameterization of the atmosphere and forest canopy through measurement of sky-view fraction (Essery et al., 2008; Sicart et al., 2006; Webster et al., 2016). This is beneficial as uncertainty in measured sky-view fraction can be well constrained experimentally at a point using hemispherical photography (Jonas et al., 2020) and related to canopy parameters more commonly used in Earth System Models to describe forest biomass, for example, effective leaf area index (Musselman et al., 2012). However, a range of additional canopy parameters are often used in models, for example, plant area index, stem area index, canopy height, and multiple in situ methods are used to quantify canopy structure, for example, destructive sampling, allometric relationships using diameter of trunks at chest height, photogrammetry, laser scanning, and so on. Consequently, model evaluation requires both constrained experimental uncertainty in point measurements and an appreciation of uncertainties linking measured canopy metrics to modelled canopy parameters.

Where sky-view fraction is a well-constrained parameter in a two-component model, remaining model uncertainties occur when estimating temperatures of down-facing canopy elements. Temperature measurements of individual canopy elements using contact thermocouples and infrared sensors, which often show strong solar heating in discontinuous forest canopies (Musselman & Pomeroy, 2017; Pomeroy et al., 2009; Rowlands et al., 2002; Webster et al., 2016, 2017), provide valuable insights into emitting temperatures of down-facing canopy elements. However, making broad, spatially distributed temperature measurements of all down-facing canopy elements using up-facing infrared imagers remains challenging, as mixed pixels combining sky and trees prevent temperature measurements solely of the canopy.

Without independent measurements of down-facing canopy temperatures, an assumption is sometimes made that the canopy is in equilibrium with air temperatures (Essery et al., 2008; Lawler & Link, 2011). In the vertical air temperature profile (below, within or above forest canopy), above canopy air temperatures are simulated prognostic variables in Earth System Models or driving data in offline snow-physics models. Similarities between above canopy air temperatures and calculated emitting canopy temperatures have previously been shown (Pomeroy et al., 2009; Sicart et al., 2004), while Webster et al. (2016) also demonstrated that above-canopy air temperatures provided the best proxy for canopy temperatures despite below-canopy air temperatures being consistently cooler. Cooler below-canopy air temperatures occur as near-surface lapse rates often strongly diverge from lapse rates of the free atmosphere; shallow air temperature inversions are common when radiative energy loss from the snow surface causes cold air to pool (Lundquist et al., 2008). This divergence may be enhanced through decoupling of near-surface and above-canopy air by frictional resistance of relatively dense, poorly ventilated forest canopies which reduces vertical turbulent mixing of air (Link & Marks, 1999). How frequent are cold air pooling and decoupling of air above and below the canopy, and how influential they are on down-facing emitting canopy temperatures, are uncertain.

The influences of boreal forests and snow cover on land surface energy balance have been of long-standing interest for numerical weather prediction and climate modelling (e.g., Thomas & Rowntree, 1992; Viterbo & Betts, 1999). Land surface models for such applications rely on simple characterizations of forest structure (typically forest fraction, canopy height and leaf area index averaged over large model grid boxes) but have high meteorological input data requirements (including shortwave and longwave radiation fluxes, air temperature and humidity, precipitation and wind speed on sub-daily timesteps). Whether provided by atmospheric models or measurements, above-canopy meteorological variables are required. In models that calculate separate energy and mass balances for forest canopies and underlying ground, surface, and canopy temperatures are prognostic variables.

To improve simulations of boreal late-winter energy exchanges between the atmosphere and the land surface, in this study we ask what impact does uncertainty in (a) canopy parameterization, and (b) emitting temperature of the down-facing canopy have on the simulation of sub-canopy longwave radiation? Consequently, we (a) evaluate how well a simple model of sub-canopy longwave emission works across a range of coniferous and deciduous boreal forest plots at two Fennoscandian study sites, (b) assess the model sensitivity to uncertainty in canopy cover, solar heating of the canopy and height of air temperature measurements, and (c) consider the impact on

Table 1
Locations, Dates and Times of Data Collection; Qualitative Descriptions and Ranges of Sky View Fractions Calculated at the Positions of the LW Sensors for Each Site

Location	Site	Start	End	Description	SVF range
Abisko 2011	Open	7 March, 14:55	5 April, 08:20	Open meadow area	–
	C	8 March, 15:05	5 April, 08:55	Medium density, mixed trees	0.52–0.90
	R1	10 March, 14:15	16 March, 12:00	Low density, small thin trees, windward forest edge	0.73–0.97
	R2	16 March, 14:30	22 March, 10:20	Low-medium density, mixed-size trees, leeward forest edge	0.63–0.96
	R3	22 March, 13:45	30 March, 11:55	High density, tall thin trees	0.43–0.60
	R4	30 March, 14:45	5 April, 10:50	Medium-high density, large polycormic trees	0.43–0.75
Sodankylä 2012	Open	8 March, 12:30	25 April, 15:55	Top of meteorological tower	–
	C	8 March, 11:30	25 April, 09:10	High density, tall pine trees	0.36–0.42
	R1	8 March, 13:45	15 March, 11:20	Low density, small pine trees	0.51–0.89
	R2	16 March, 08:40	22 March, 10:35	High density, medium pine trees	0.45–0.48
	R3	23 March, 15:55	31 March, 08:55	Medium density, mainly spruce but with some birch and pine	0.28–0.57
	R4	31 March, 12:35	16 April, 04:35	Low density, large pine, birch and spruce trees	0.29–0.56

model performance of temperature inversions in stable atmospheric conditions decoupling canopy temperatures and above-canopy air temperatures. The ability of a land surface model to predict sub-canopy longwave radiation when driven with above-canopy meteorology is discussed.

2. Study Sites

Measurements were made at two study sites in northern Sweden (March–April 2011) and Finland (March–April 2012). The Abisko study site (68.32°N, 18.83°E) was located approximately 3 km south of Abisko village. The Sodankylä study site (67.36°N, 26.63°E) was located at the Arctic Research Center of the Finnish Meteorological Institute (FMI). Solar elevation at solar noon ranged between 18.0 and 27.7° at Abisko and 18.8–31.5° at Sodankylä during the study periods. At each site, five 20 × 20 m plots (see Table 1 for plot locations, descriptions and measurement durations) were chosen to represent a breadth of canopy structural characteristics (e.g., height, density) and range of sky view fractions. At each site, continuous sub-canopy longwave measurements were made at plot C for the entire study period, while a separate roving array of sensors was moved between plots R1 and R4 (see Figure 1 in Reid et al. (2014) for summer aerial photos of sites and locations of plots).

At Abisko, the five plots were located across a 250 m extent in discontinuous forest close to treeline, dominated by polycormic downy birch (*Betula pubescens* Ehrh.). At Sodankylä, the five plots were located across a 1 km extent within a partially managed forest. Scots pine (*Pinus sylvestris* L.) dominated plots C and R1, plot R3 was dominated by spruce (*Picea abies* (L.) Karsten), and plot R4 had a mix of Scots pine, spruce and silver birch (*Betula pendula* Roth). See Appendix A for all measurements.

3. Methods

3.1. Meteorology

Air temperatures at 0.5 m above the snow surface were measured in each plot in Abisko and Sodankylä. At Sodankylä, air temperatures were measured at additional heights on a tower located 200 m south east of R1: within the canopy at 3 m and above the canopy at 18 m; the average tree height around the tower was 12 m (Kangas et al., 2016). Above-canopy radiation measurements (longwave, total incoming shortwave, and diffuse shortwave fraction) were made from a tower above the trees at Sodankylä and at the highest point in the open meadow site at Abisko, which best approximated above-canopy conditions in lieu of a tower being available. An overview of all instrumentation specifications can be found in Table 2.

Beneath the forest canopy, four longwave sensors within each plot (four in plot C and four in the roving array moved between plots R1–R4) were placed on small plywood platforms on top of the snowpack and were manually

Table 2
Instrument Specifications for Meteorological and Tree Temperature Instrumentation (fov = Field of View)

Variable (spectral range)	Manufacturer	Instrument	Accuracy (sensitivity/fov)	Measurement frequency
SW radiation (0.3–2.8 μm)	Kipp & Zonen	CMP3	±10% (5–20 μV Wm^{-2}/180°)	5 s samples averaged to 5 min
LW radiation (4.5–42.0 μm)	Kipp & Zonen	CGR3	±10% (5–15 μV Wm^{-2}/150°)	5 s samples averaged to 5 min
Total and diffuse SW radiation (0.4–0.7 μm)	Delta-T devices	BF3 sunshine sensor	Total: ±12%Diffuse: ±15%	5 s samples averaged to 5 min
Air temperature (0.5 m above snow surface)	Vaisala	WXT 520	±0.3°C	60 s samples averaged to 5 min
Air temperature (18 m above ground)	Pentronic	PT100	±0.3°C	Hourly averages
Tree surface temperature - direct	RS Components	Type-T thermocouples (Copper/Constantan)	±1°C	5 s samples averaged to 5 min
Thermal Imagery (7.5–13 μm)	FLIR	B620	±2°C or 2% (fov: 24° × 18°)	Occasional samples

leveled each day. The four sensors were located to capture sky view fractions representative of the full range measured at 10 positions in each plot (Table 1) and trunk-heating characteristics. This range was captured by locating two sensors within 0.5 m north and south of a tree trunk, and the other two sensors in relatively open and closed sections of the canopy.

Before deployment at Sodankylä, the longwave sensors were compared side by side for 8 hours with a good view of the sky from the frozen Kitinen River. The range between sensors was ±3.2 W m^{-2} or ±1.5%. During each measurement campaign, plots were visited once or twice per day to manually clean and level the longwave sensors. Measurements at both sites then underwent rigorous quality control to discard data where sensors had been occluded by snow or frost, had tilted to unacceptable levels or where values were unrealistic; see appendix B in Reid et al. (2014) for further details.

3.2. Forest Canopy Temperature and Sky View Fraction

Pairs of type T contact thermocouples, consisting of copper and constantan conductors, were embedded within the tree trunk bark through small incisions, approximately one or 2 mm from the surface. Sixty-four thermocouple pairs were inserted into single trees at Abisko C, Sodankylä C, and Sodankylä R4. Thermocouples were used in pairs at each position on the tree trunk to identify and remove faulty measurements. Mean values of thermocouple pairs were subsequently calculated for each 5-min timestep at each trunk position (11 March to 5 April 2011 in Abisko, 10 March to 12 April 2012 in Sodankylä), between 5 and 150 cm above the snow surface in north- and south-facing directions.

A FLIR B620 thermal camera was used to take images (640 × 480 resolution, camera positioned ∼2 m away from tree) of a west-facing pine tree trunk in Sodankylä R4. Snapshot measurements were made periodically throughout the Sodankylä R4 measurement period to assess spatial variability of tree trunk temperatures at sub-centimeter resolution.

Sky view fraction was characterized by hemispherical photographs taken 30 cm above the snow surface during overcast conditions using a Nikon Coolpix 4300 digital camera with a Nikon FC-E8 fisheye converter lens. Reid et al. (2014) provides further detail of the techniques to create sky view fraction from raw hemispherical images, accounting for canopy and sky thresholding, and processing considerations following Essery et al. (2008). Additionally, in the Abisko birch forest, light colored bark created reflective trunk sections and leafless canopies caused free-flying branch elements; a branch-joining algorithm was employed to correct errors (Reid & Essery, 2013).

The range of sky view fractions in each 20 × 20 m plot were characterized at 10 locations distributed on a regular grid, plus the sky view fractions at the positions of the four longwave sensors. At Abisko, sky view fractions ranged between 0.43 and 0.97, while at Sodankylä sky view fractions ranged between 0.28 and 0.89, but clustered between 0.28 and 0.57. High sky view fractions at Abisko reflected the broadleaved deciduous (leaf-off) and sparse nature of the canopy, while lower sky view fraction at Sodankylä reflected the largely coniferous needleleaved (evergreen) canopy.

3.3. Models

The next section presents results from empirical and physical models of sub-canopy downwelling longwave radiation. The simplest model just uses above-canopy longwave radiation, air temperature and sky view fraction as inputs. Improvements in the performance of this model by calibrating sky view fraction or including above-canopy shortwave radiation as a predictor are evaluated, and the impacts of using either sub-canopy or above-canopy air temperatures are investigated. FSM2, a multi-physics snow model (Essery, 2015) coupled with a forest canopy model (see Appendix A in Mazzotti, Essery, Moeser, & Jonas, 2020), is taken as an example of a physical land surface model. Here, FSM2 is tested at Sodankylä, where its application is enabled by the high level of permanent instrumentation operated by FMI and the collation of a complete driving dataset for such models by Essery et al. (2016). The configuration of FSM2 used is of typical complexity for current land surface models and represents the canopy as a single model layer, uses Beer's Law for radiative transfer through the canopy, has a canopy heat capacity proportional to

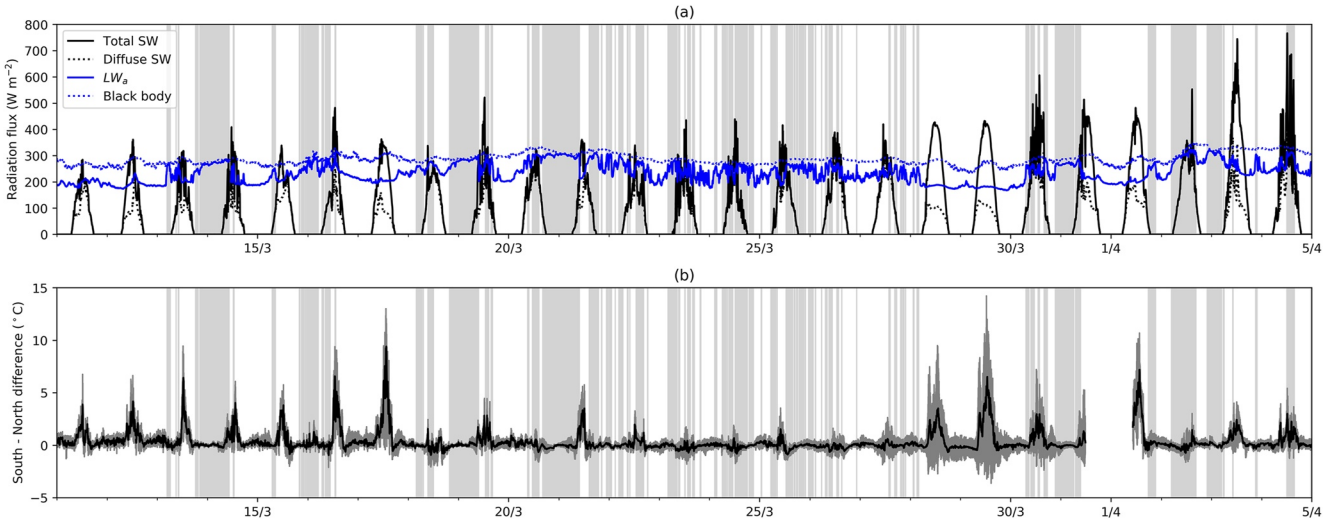

Figure 1. (a) Above-canopy downwelling total shortwave, diffuse shortwave and longwave radiation fluxes measured at Abisko in March-April 2011. Black body radiation is calculated from air temperatures measured in the open meadow. Gray bands indicate cloudier periods with apparent atmospheric emissivity greater than 0.9. (b) Average (black lines) and range (dark gray bands) of differences in tree trunk temperatures (South–North) measured using contact thermocouples.

vegetation area index and adjusts turbulent fluxes between the canopy and the atmosphere according to atmospheric stability.

4. Results

Figure 1a for Abisko and Figure 2a for Sodankylä show above-canopy downwelling fluxes of longwave and shortwave radiation, along with the potential longwave radiation estimated as blackbody radiation at the above-canopy air temperature. An apparent atmospheric emissivity can be defined as

$$\varepsilon_a \equiv \frac{LW_a}{\sigma T_a^4} \tag{1}$$

where LW_a (W m^{-2}) is downwelling longwave radiation from the atmosphere, σ is the Stefan-Boltzmann constant (5.67×10^{-8} W m^{-2} K^{-4}) and T_a (K) is air temperature. LW_a and ε_a increase when the sky is cloudy. Values of ε_a calculated from measurements in the meadow at Abisko and above the canopy at Sodankylä range between 0.6

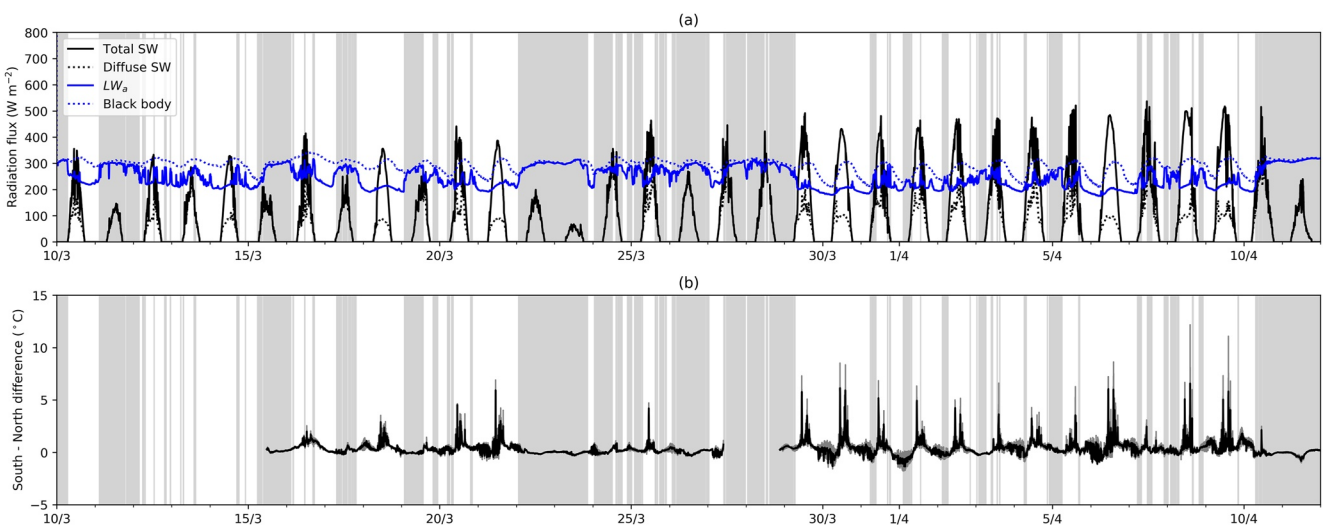

Figure 2. As Figure 1, but for Sodankylä in March–April 2012.

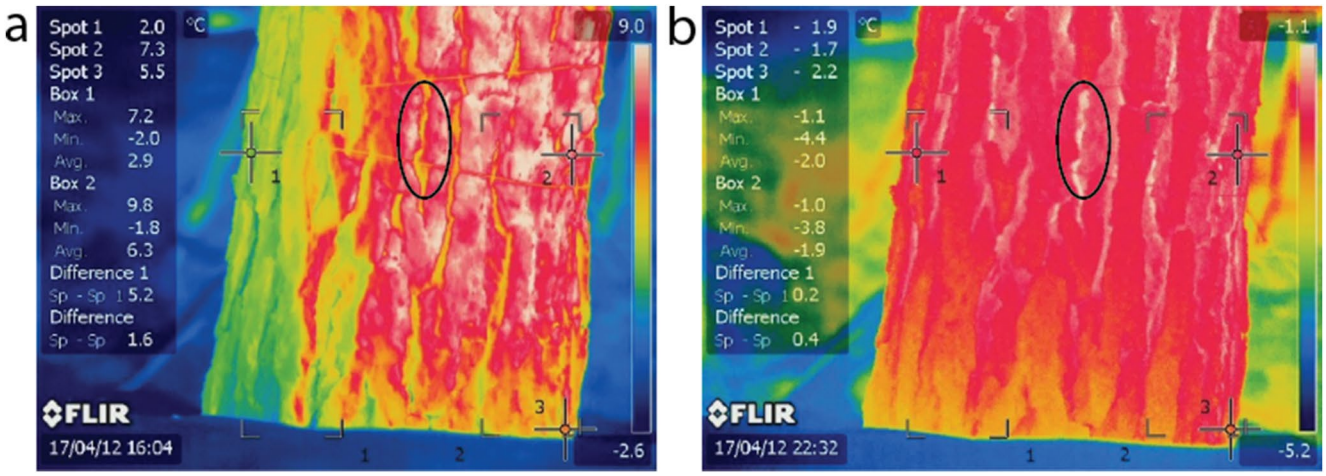

Figure 3. Infrared thermal photographs of west-facing pine bark on 17 April 2012 at: (a) 16:04 showing effect of direct solar heating on the south (right hand) side of the trunk (air temperature at 0.5 m was 1.6°C) and (b) 22:32, 1 hr and 20 min after sunset, showing retention of warmer air within crevices (air temperature at 0.5 m was −1.7°C). Note different color scales on right hand side (°C), rectangular boxes are delineated using corners, positions of spot temperatures are shown by cross-hairs, and black ovals highlight cracks in bark which are relatively cool during day and warm at night.

and 1, and gray bands in Figures 1 and 2 mark periods with $\varepsilon_a > 0.9$. These correspond well with cloudy daytime periods when the measured incoming shortwave radiation was mostly diffuse but also allow identification of cloudy conditions at night (see Appendix Figure A1 for above and below canopy longwave measurements from all individual sensors).

Forest materials have high thermal emissivity (Lundquist et al., 2018), and multiple scattering of longwave radiation beneath the canopy increases the apparent emissivity toward 1 (akin to cavity radiation). Assuming $\varepsilon_c = 1$ simplifies calculations by removing multiple reflections. Sub-canopy downwelling longwave radiation (LW_s) then simply comprises longwave radiation emitted from the canopy and the fraction of LW_a from the atmosphere that passes through canopy gaps. Different parts of the canopy can have widely differing temperatures, but an effective canopy temperature T_c can be defined as the temperature satisfying

$$LW_s = (1 - f_v)\sigma T_c^4 + f_v LW_a, \tag{2}$$

where f_v is the hemispheric sky view fraction from under the canopy.

Canopy temperature differences are illustrated by measured tree trunk temperatures. Mean hourly temperature differences between south and north faces of tree trunks at Abisko (Figure 1b) and Sodankylä (Figure 2b) showed increased south-facing warming in response to solar heating, often varying diurnally between 0 and 5°C and often exceeding 5°C on cloud-free days. For a pine tree in Sodankylä R4, Figure 3 illustrates that while the diurnal heating of south facing trunks was a robust pattern, temperatures could be highly spatially variable. During the day, while spot measurements were 5.2°C warmer on the south-facing side of the trunk, high spatial variability in trunk surface temperature was evident; warming was highest on plates of the protruding outer bark surface, with cooler areas in vertical cracks (ovals in Figure 3 highlight cracks). At night, spot measurements showed that the south-facing temperature difference reduced to 0.2°C, and the warmest areas of bark were the vertical cracks relative to the cooler outer surface. Throughout the diurnal cycle, cooling was evident where the bark surface was adjacent to the cold snow surface.

While patterns of trunk surface temperatures beneath the forest canopy were spatially and temporally complex, mean differences between thermocouple temperatures of tree trunks and near-surface (0.5 m) sub-canopy air temperatures showed trunks were 0.7–1.2°C warmer than air temperatures in coniferous and mixed plots in Sodankylä and 1.5°C warmer than air temperatures in deciduous birch in Abisko. This disconnect between trunk and sub-canopy air temperatures was evident for example, clear sky days in the C plots at both locations (Figure 4), with trunk temperatures showing effects of sun flecks during the day and heat storage at night. Within-canopy air temperatures, measured at Sodankylä only, were closer to the trunk temperatures and revealed strong inversions near the snow surface at night. Effective canopy radiative temperatures (obtained by inverting Equation 2 using

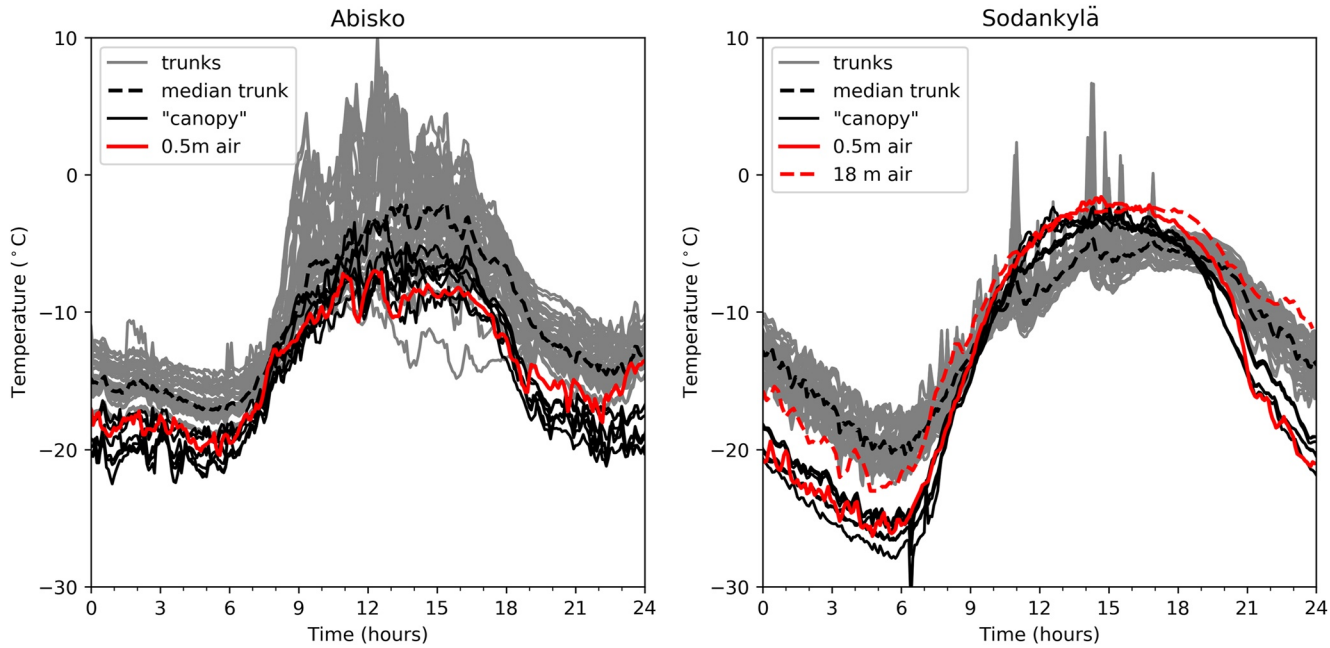

Figure 4. Air temperatures, trunk temperatures and apparent canopy radiative temperatures obtained by inverting Equation 2 for clear-sky days 29 March 2011 at Abisko and 6 April 2012 at Sodankylä.

measured LW_s, LW_a and f_v) more closely followed sub-canopy air temperatures. Hence, we hypothesize that the shaded and ventilated underside of a canopy would be close to equilibrium with sub-canopy air temperature. This is supported by high correlations between sub-canopy longwave radiation and sub-canopy air temperature (Figure 5), especially for dense canopies ($f_v < 0.5$). Correlation of longwave radiation above and below the canopy should clearly approach 1 as f_v tends toward 1, but correlations with sub-canopy air temperature and shortwave radiation do not approach zero. Downwelling radiation from the atmosphere depends on humidity and cloud cover in addition to air temperature (indeed, air temperature, humidity and cloud cover measurements are often used to predict downwelling longwave radiation when direct measurements are not available). There can be a negative correlation between downwelling longwave and shortwave radiation for $f_v = 1$ because of increased longwave radiation and decreased shortwave radiation in overcast conditions. Positive correlations of sub-canopy longwave radiation with above-canopy shortwave radiation are seen in Figure 5 for denser canopies, but they are consistently smaller than correlations with sub-canopy air temperature.

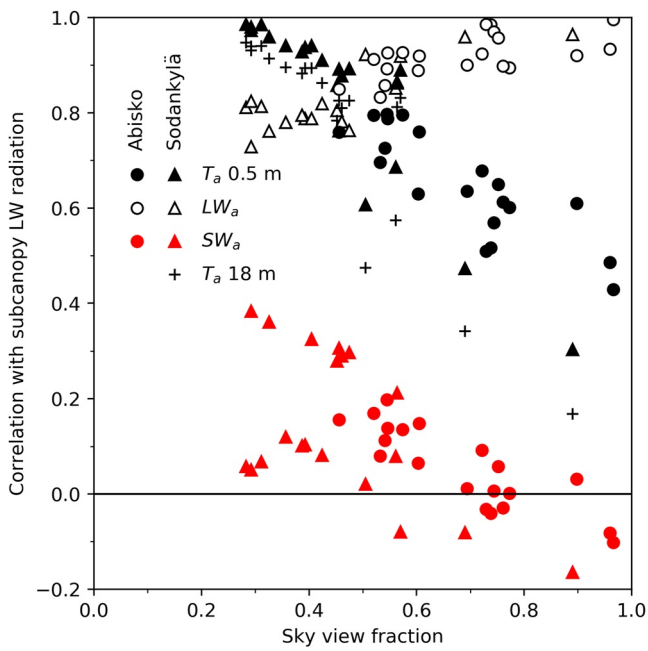

Figure 5. Correlation of sub-canopy (0.5 m) air temperature, above-canopy longwave radiation and above-canopy shortwave radiation with sub-canopy longwave radiation measured by each radiometer at Abisko and Sodankylä. Correlation of above-canopy (18 m) air temperature and sub-canopy longwave radiation can be calculated at Sodankylä only.

Because the apparent atmospheric emissivity will be less than one except in overcast conditions, the presence of a canopy generally increases longwave radiation at the surface, even when the canopy temperature does not exceed the above canopy air temperature. Defining a canopy longwave enhancement factor

$$e_c \equiv \frac{LW_s}{LW_a}, \tag{3}$$

Equations 1, 2 and the assumption $T_c = T_a$ give

$$e_c = 1 + \left(\varepsilon_a^{-1} - 1\right)(1 - f_v). \tag{4}$$

Figure 6 compares this function with measurements of e_c averaged over the four radiometers in each plot at Abisko and Sodankylä. The measurements

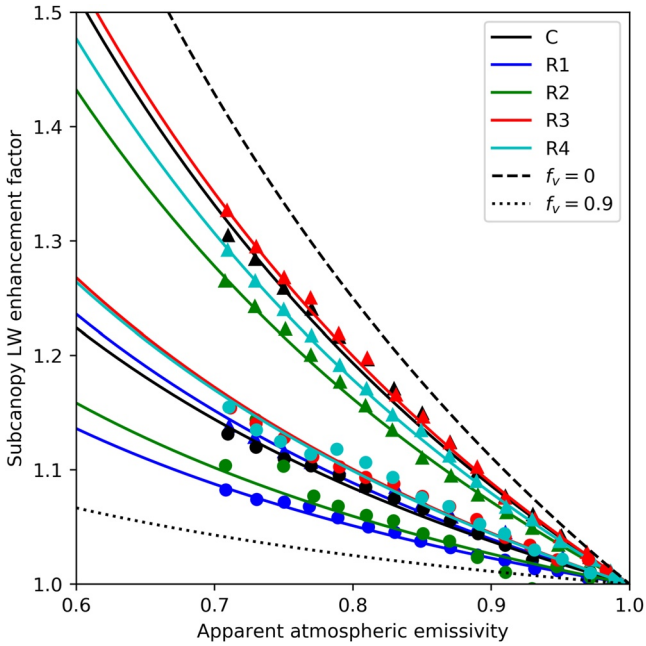

Figure 6. Sub-canopy longwave enhancement factors calculated from averages over the four radiometers in each plot at Abisko (circles) and Sodankylä (triangles), binned according to apparent atmospheric emissivity. Lines are given by Equation 4 with fitted or specified sky view fractions.

have been binned into ranges of ε_a determined from measurements of LW_a and above-canopy T_a. Equation 4 can be fitted to the measurements for each plot by adjusting f_v. The ε_a^{-1} dependency suggests that longwave enhancement occurs even for sparse canopies under clear skies.

High correlations of sub-canopy longwave radiation with sub-canopy air temperature for dense canopies and with above-canopy longwave radiation for sparse canopies suggest that Equation 2 with $T_c = T_a$ can give good estimates of sub-canopy longwave radiation for all homogeneous canopy densities, provided that sky view fractions are measured accurately. High correlation and low biases (less than ± 9 W m^{-2}) are evident between average sub-canopy longwave radiation measurements and estimates from Equation 2 with the assumption $T_c = T_a$ (Figure 7). There is a clear tendency for underestimation of sub-canopy longwave radiation enhancement for the Sodankylä measurements, but not for Abisko, and only a few predictions are outside the sensor calibration uncertainty.

Errors in measured sky view fractions are a possible source of error in predictions with Equation 2. Hemispherical photographs were taken under variable sky conditions and binarized using manually chosen brightness thresholds, so the measured sky view fractions are quite uncertain. Biases in Equation 2 can be removed by replacing the measured sky view fractions with

$$f_v = \left(\overline{\sigma T_a^4 - LW_s}\right)\left(\overline{\sigma T_a^4 - LW_a}\right)^{-1} \quad (5)$$

for each radiometer, where bars denote averages over the measurement periods. This fitting shows no clear bias in f_v for Abisko, but it consistently decreases f_v for the denser canopies at Sodankylä (Figure 8a). Removing biases also decreases root mean square errors in sub-canopy longwave radiation predictions (Figure 8b). Bias removal does not give an independent method of predicting sub-canopy longwave radiation, because the

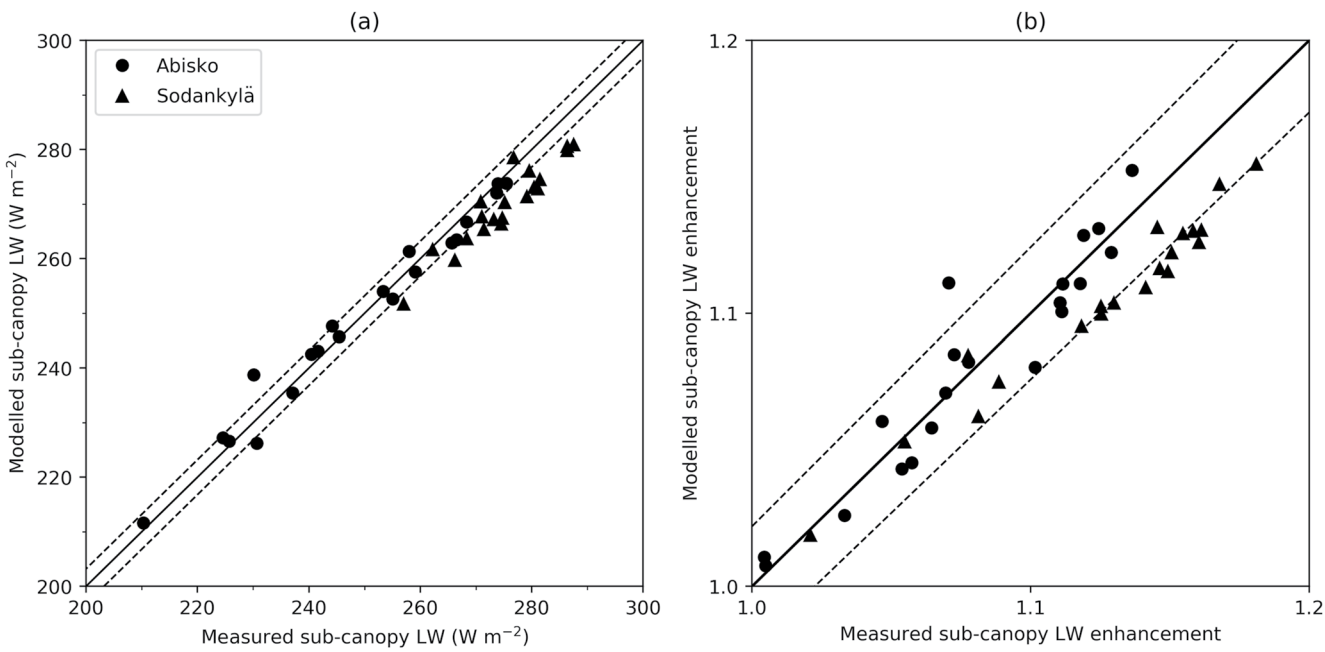

Figure 7. Sub-canopy (a) longwave radiation and (b) longwave enhancement measured by each radiometer at Abisko and Sodankylä and predicted by Equation 2 with sub-canopy air temperature, averaged over the measurement periods. Dashed lines show the ±1.5% spread found by comparison of the radiometers, combined in quadrature for LW enhancement ratios.

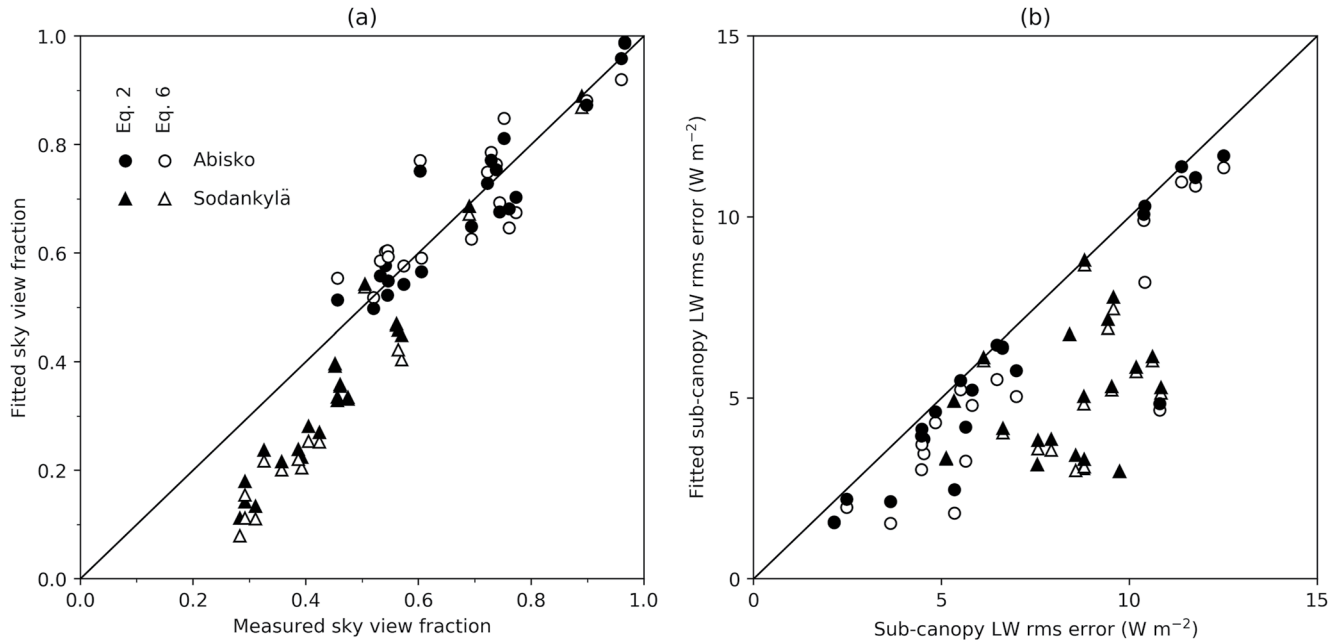

Figure 8. Comparisons of (a) measured and fitted sky view fractions, and (b) errors in sub-canopy longwave radiation predicted with measured and fitted sky view fractions. Filled symbols show results obtained by adjusting sky view fraction to remove biases in predictions with Equation 2; open symbols show results obtained by minimizing rms errors in predictions with Equation 6 by multiple linear regression.

measurements were used in Equation 5, but it gives an indication of the irreducible error in using Equation 2 to make predictions.

Essery et al. (2008) found that predictions of sub-canopy longwave radiation for a forest on a southeast-facing slope and in a forest gap could be improved by including measured above-canopy shortwave radiation SW_a as a predictor. For the level and continuous forest stands studied at Abisko and Sodankylä, replacing Equation 2 with

$$LW_s = \sigma T_a^4 + f_v\left(LW_a - \sigma T_a^4\right) + f_s SW_a \quad (6)$$

and fitting the coefficients f_v and f_s to sub-canopy longwave radiation measurements using multiple linear regression gives only small reductions in errors (Figure 8b) compared with using above-canopy longwave radiation and sub-canopy air temperature as predictors.

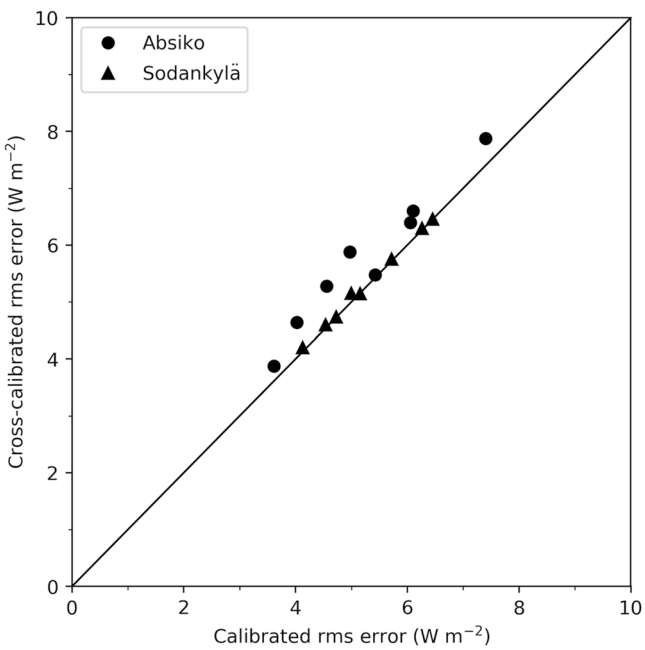

Figure 9. Comparison of errors in sub-canopy LW radiation fitted to measurements and using sky view fractions fitted to independent calibration periods for C radiometers at Abisko and Sodankylä.

Evaluation of results requires measurements over a period with varying sky conditions to give a large range in sub-canopy LW radiation. The R radiometers were only in fixed positions for a few days at a time, but the C radiometers were in position long enough for the measurements to be split into calibration and evaluation periods. After quality control, 450 hr of data remain for the four C radiometers at Abisko and 800 hr at Sodankylä. Equation 5 was used to fit a sky view fraction to half of the data for each radiometer and the fitted sky view fraction was then used in Equation 2 with the calibration data to find the calibrated rms error and with the evaluation data to find the cross-calibrated error. Each period was used for both calibration and evaluation in turn for the four radiometers and two sites, giving the 16 points in Figure 9. Transfer of fitted sky view fractions to evaluation periods increases rms errors by less than 1 W m^{-2} at Abisko, well within the measurement uncertainty. Calibrated and cross-calibrated errors are almost identical at Sodankylä.

There can be strong vertical air temperature gradients near the ground, driven by shortwave radiative heating of the surface during the day and longwave

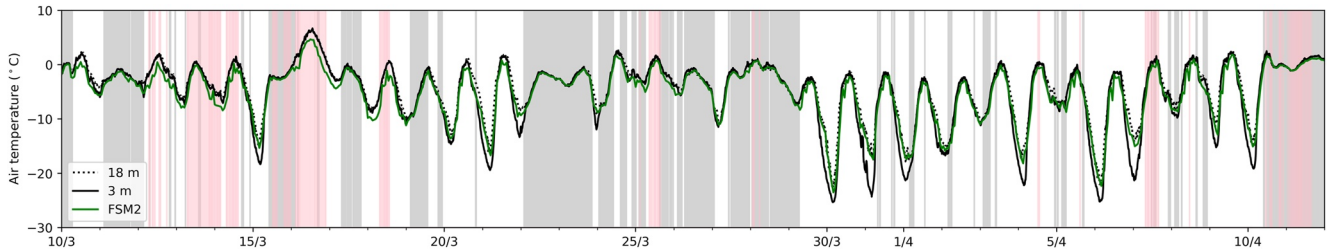

Figure 10. Air temperatures measured at 3 and 18 m heights within and above the forest canopy at Sodankylä during the 2012 study period. The green line is within-canopy air temperature simulated by FSM2. Gray bands show periods of cloud cover diagnosed by comparing blackbody radiation at the above-canopy air temperature and actual incoming longwave radiation above the canopy. Pink bands show periods with 18 m wind speed exceeding 4 m s^{-1} ("gentle breeze: leaves and small twigs in constant motion" on the Beaufort scale).

radiative cooling at night. Air temperatures above and below forest canopies are further modified by exchanges of heat with the forest biomass. Measured air temperatures above and within the canopy at Sodankylä (Figure 10) often diverged at night during the study period (above-canopy air temperatures were unavailable at Abisko). Air temperatures below the canopy never exceeded those above by much because convection mixes the air efficiently in unstable situations, but air temperatures below the canopy commonly fell several degrees lower than those above on clear and calm nights ($\varepsilon_a < 0.9$ and wind speed less than 4 m s^{-1}). Variations from day-to-day are strongly influenced by advection of air masses, for example, the passage of a warm sector on 16-17 March in Figure 10, but more frequent and stronger inversions are expected in the late-winter months, whereas superadiabatic lapse rates (<−0.0098°C m^{-1}) are more common in summer. This is confirmed by seasonal temperature gradient statistics in Figure 11 calculated from 10 years of hourly measurements at Sodankylä. Diurnal temperature ranges were greater nearer to the ground and tended to increase as the apparent emissivity of the atmosphere decreased (Figure 12), allowing more shortwave heating and longwave cooling.

Assuming that the majority of downward longwave radiation beneath the canopy is emitted by biomass in the lower canopy that is in contact with the below-canopy air, it should be more strongly influenced by the sub-canopy air temperature. Measured sub-canopy longwave radiation at Sodankylä had stronger correlations with below-canopy than above-canopy air temperatures (Figure 13a), particularly due to differences in minima at night (Figure 10). Consequently, lower root mean squared errors were obtained (Figure 13b) using below-canopy

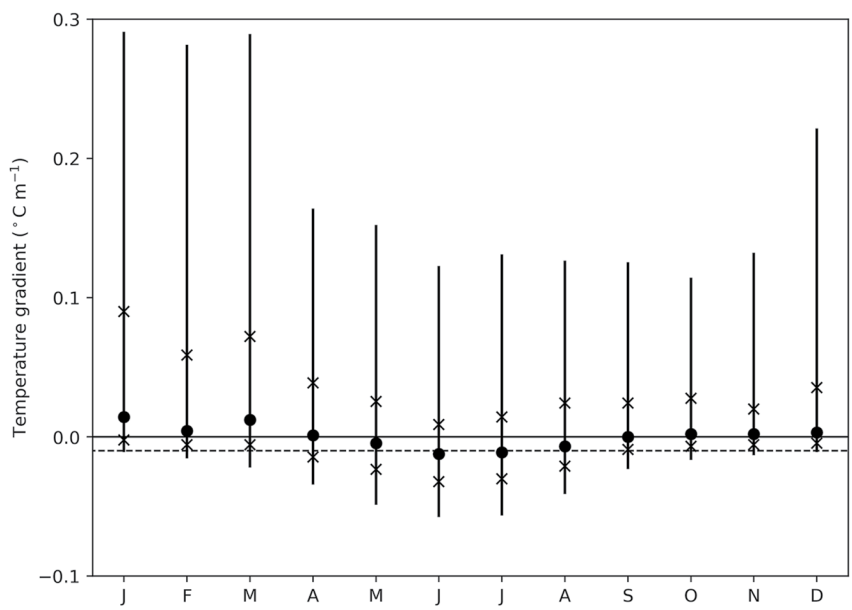

Figure 11. Monthly median (dots), interquartile range (crosses) and 5–95 percentile range (bars) for hourly average air temperature gradients between 3 and 18 m heights measured at Sodankylä from 2011 to 2020. The dashed line shows the dry adiabatic lapse rate.

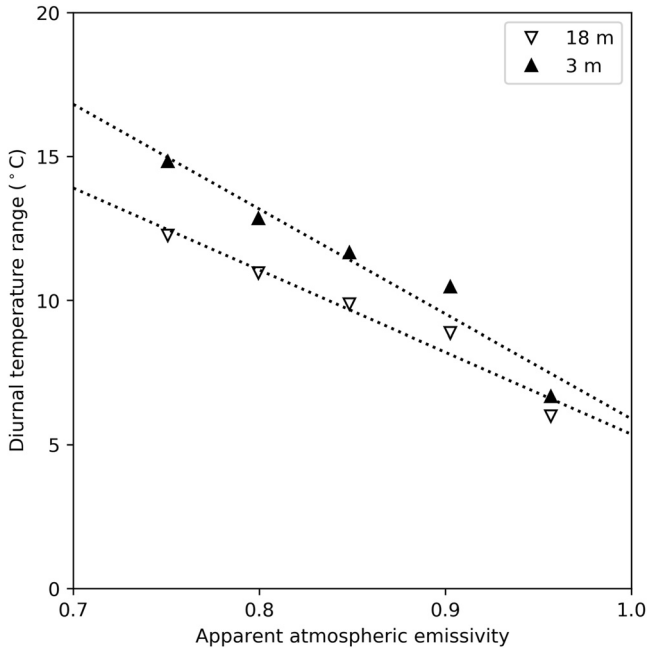

Figure 12. Average diurnal air temperature ranges within and above the canopy at Sodankylä in March, binned according to apparent atmospheric emissivity. Dotted lines were fitted by linear regression.

air temperatures in Equation 2 after removing biases by fitting sky view fractions using Equation 5. However, while below-canopy air temperature measurements are easy to make during field experiments, they are not widely available otherwise; the World Meteorological Organization standard is that near-surface air temperature measurements should be made in open locations and not shaded by trees.

Above-canopy air temperatures are only available at sites like Sodankylä with instrumented masts, but they are required as inputs to land surface energy balance models for forest simulations (Rutter et al., 2009). In addition to empirical model errors, Figure 13b also shows errors in sub-canopy longwave radiation for FSM2 driven with above-canopy meteorology and sky view fractions from Equation 5 but no further calibration. The FSM2 errors are consistently smaller than errors for Equation 2 with above-canopy air temperature, and even smaller than errors for Equation 2 with below-canopy air temperature for a few of the Sodankylä radiometers. In common with other land surface models, FSM2 decreases coupling between canopy and above-canopy temperatures in stable conditions, and is therefore better able to represent low below-canopy longwave radiation on clear, calm nights. Within-canopy air temperature is a state variable in FSM2 and can be compared with measurements at Sodankylä. Figure 10 shows that the simulated within-canopy air temperature can fall below the driving above-canopy air temperature in stable conditions but does not fall as low as the measured within-canopy temperature. A model sensitivity study in Appendix B shows that within-canopy air temperature is strongly dependent on wind speed and decoupling in very stable conditions.

We have used several models to predict sub-canopy longwave radiation; Table 3 summarizes the average rms errors for these models at Abisko and Sodankylä. Equation 2 with measured sky view fraction and measured sub-canopy air temperature gave errors less than 9 W m^{-2} for both sites. Adjusting the sky view fraction for each radiometer to remove biases decreased rms errors. A multiple regression driven with measured sub-canopy

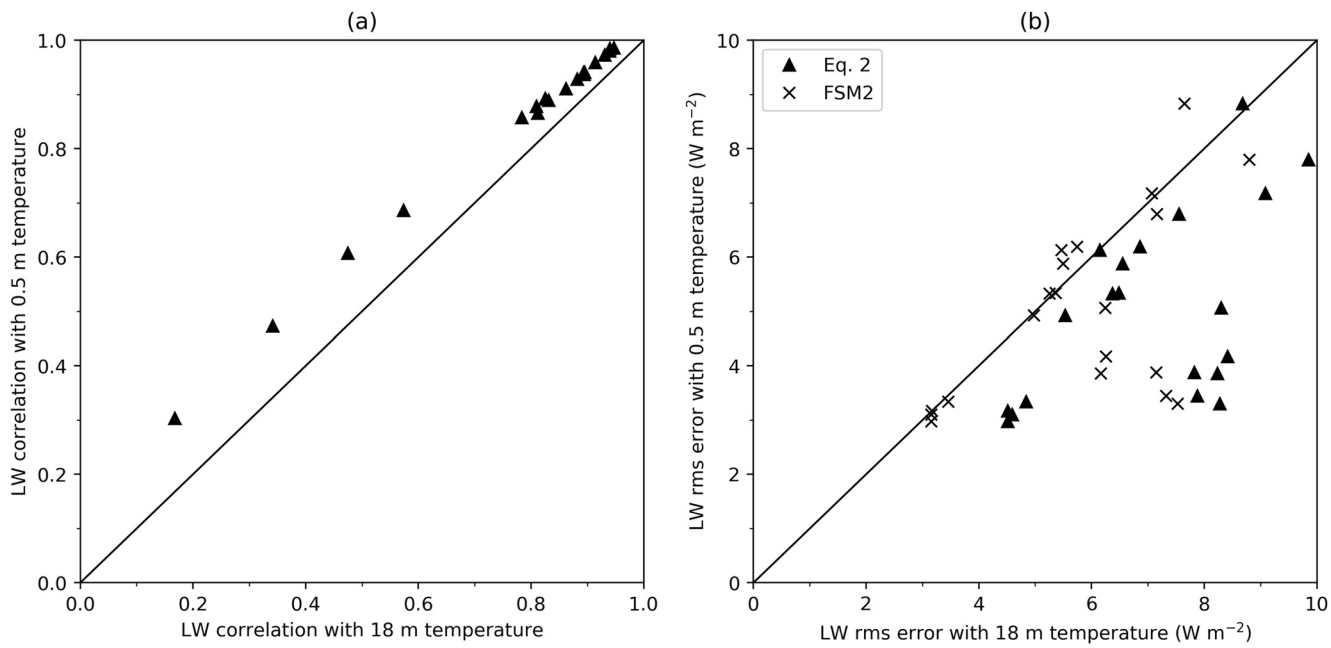

Figure 13. (a) Correlation of sub-canopy longwave radiation measured by each radiometer at Sodankylä with air temperatures measured below and above the canopy. (b) Errors in sub-canopy longwave radiation predicted with sub-canopy air temperatures and fitted sky view fractions compared with errors obtained using above-canopy air temperatures in either Equation 2 or FSM2.

Table 3
Average rms Errors for Sub-Canopy LW Radiation at Abisko and Sodankylä Predicted With Equation 2, Equation 6 or FSM2, Driven With Sub-Canopy or Above-Canopy Air Temperatures, and With No Fitting, Fitted f_v or Fitted f_v and f_s

Model	T_a height	Fitting	Abisko	Sodankylä
Equation 2	0.5 m	–	6.8 W m^{-2}	8.4 W m^{-2}
Equation 2	0.5 m	f_v	5.9 W m^{-2}	5.0 W m^{-2}
Equation 6	0.5 m	f_v, f_s	5.4 W m^{-2}	4.9 W m^{-2}
Equation 2	18 m	f_v	–	7.0 W m^{-2}
FSM2	18 m	f_v	–	5.8 W m^{-2}

air temperatures and above-canopy SW radiation gave a further but smaller reduction in errors. The additional meteorological measurements provided by FMI at Sodankylä allowed us to test predictions using air temperatures measured above the canopy and with a forest canopy model. The error for Equation 2 driven with above-canopy air temperature was larger than with sub-canopy temperature, even after fitting the sky view fraction to remove biases. The canopy model in FSM2 driven with a meteorological dataset including above canopy air temperature decreased this error.

5. Discussion and Conclusions

Sub-canopy longwave radiation is often a dominant component of boreal late-winter energy exchanges. In this study, we have shown that uncertainty in canopy density is a primary control on uncertainty in simulations of sub-canopy longwave radiation, while uncertainty in emitting temperature of the downward-facing canopy is secondary. Warming of canopy elements (trunks, branches, needles etc.) by solar radiation resulting in increased emissions of longwave radiation, colloquially referred to as "hot trees", has been the focus of recent model evaluations (Musselman & Pomeroy, 2017; Pomeroy et al., 2009; Schwartz et al., 2021; Webster et al., 2016, 2017). However, here we report the interacting influences of forest density and decoupling of canopy temperature from above-canopy air temperatures (De Frenne et al., 2021) on night-time overestimation of longwave emissions ("cold trees"), which has been subject to less scrutiny. We also observed strong near-surface inversions that decouple the snow surface from the atmosphere on clear, calm nights (Foken, 2022).

The high performance of a simple two-component longwave emission model (Equation 2), away from forest gaps and edges, reinforced the effectiveness of hemispherical sky view fraction as a measure of forest canopy structure to calculate longwave enhancement (Mazzotti et al., 2019; Todt et al., 2018). Irreducible errors remaining after removing biases using Equation 5 provided a useful guide for the overall level of uncertainty that could be expected using this modeling technique. The dominance of sky view is strengthened away from forest edges where sunlit tree trunks become less influential as the proportion of the sky obscured decreases rapidly with distance from a trunk (see Appendix C). However, any model requirement to use f_v or an effective leaf area index (Musselman et al., 2012) derived directly from hemispherical photographs can limit their potential for application on large scales. The capacity to create synthetic hemispherical images characterizing f_v from terrestrial lidar (Hancock et al., 2014) or airborne lidar (Moeser et al., 2014; Morsdorf et al., 2006) begins to address this limitation. In particular, Webster et al. (2020) showed that the use of airborne lidar in conjunction with a canopy height model performed well in evergreen needleleaf forests relative to in situ hemispherical images (f_v RMSE <0.1), which is promising for future kilometer-scale catchment applications. However, metrics related to bulk canopy density, for example, canopy closure or leaf area index, are usually used in land surface models, and model skill in simulation of energy exchange weakens in variable canopy cover (Moeser et al., 2020). Consequently, a key challenge in constraining model uncertainty remains the adequate translation of canopy parameterization for the purposes of radiative transmission and emittance in hyper-resolution (~2 m) models using f_v (Broxton et al., 2015; Mazzotti, Essery, Moeser, & Jonas, 2020; Mazzotti, Essery, Webster, et al., 2020) to Earth System Models working at degree resolutions which use bulk canopy parameterizations. This challenge was identified as a poorly constrained source of uncertainty in the SnowMIP2 intercomparison of forest snow process models (Rutter et al., 2009), and remains persistent. However, the development of effective bulk canopy parameterizations for radiative transmission and emittance (e.g., Malle et al., 2021) is now starting to provide first-order empirical solutions in lieu of more explicit solutions using canopy gap fraction.

Improved representations of canopy structure need to be accompanied by better measurements and simulation of canopy temperatures to improve simulation of sub-canopy longwave radiation further. Further improvement is challenging as measurements of downward-facing canopy element temperatures through spatially limited contact measurements or temporally limited spatial imaging currently provide an incomplete understanding of warming and cooling beneath the canopy top in heterogeneous forests. In addition, the extent of lower canopy warming and cooling is difficult to approximate from down-looking above-canopy thermal imaging due to down-facing canopy elements being self-obscured or only visible at very limited view angles. Despite these limitations, measuring vertical profiles of temperatures through forest canopies is increasingly possible using structure from motion

techniques combining optical and thermal imagery from uncrewed aerial vehicles (Webster et al., 2018). Such measurements may in future be used to capture low sub-canopy longwave emittance due to decoupling of canopy temperatures in stable conditions, which the two-component longwave model struggles to replicate adequately with above-canopy air temperatures.

Forest canopy schemes in land surface models need to simulate atmospheric decoupling between above-canopy air and canopy temperatures reliably during stable atmospheric conditions. Decoupling causes temperature inversions which are common over snow, are often intensified at night, and are further enhanced through aerodynamic resistance to vertical air movement by forest canopy elements. The atmospheric stability correction in FSM2 decreases the emitting canopy temperatures, thereby improving simulations of longwave radiation to snow during these stable atmospheric periods. This is an important addition to recent model developments, which have largely concentrated on decreasing model cold bias at night through decreasing the diurnal amplitude of simulated canopy temperature. The decrease in diurnal amplitude increases emitting canopy temperatures at night through explicit consideration of leaves and trunks in a two-layer canopy model (Gouttevin et al., 2015) or an empirical correction to a single-layer "big leaf" approach (Todt et al., 2019). While reduction of model errors through reducing the diurnal amplitude of emitting canopy temperatures is a pragmatic approach for global scale models, at high resolution, for example, 2 m hyper-resolution (Mazzotti, Essery, Webster, et al., 2020), our results show that accurate representation of night-time downward-facing canopy emitting temperatures requires careful process representation of turbulent energy exchanges affecting sub-canopy and within-canopy air temperate regimes.

Appendix A

Figure A1.

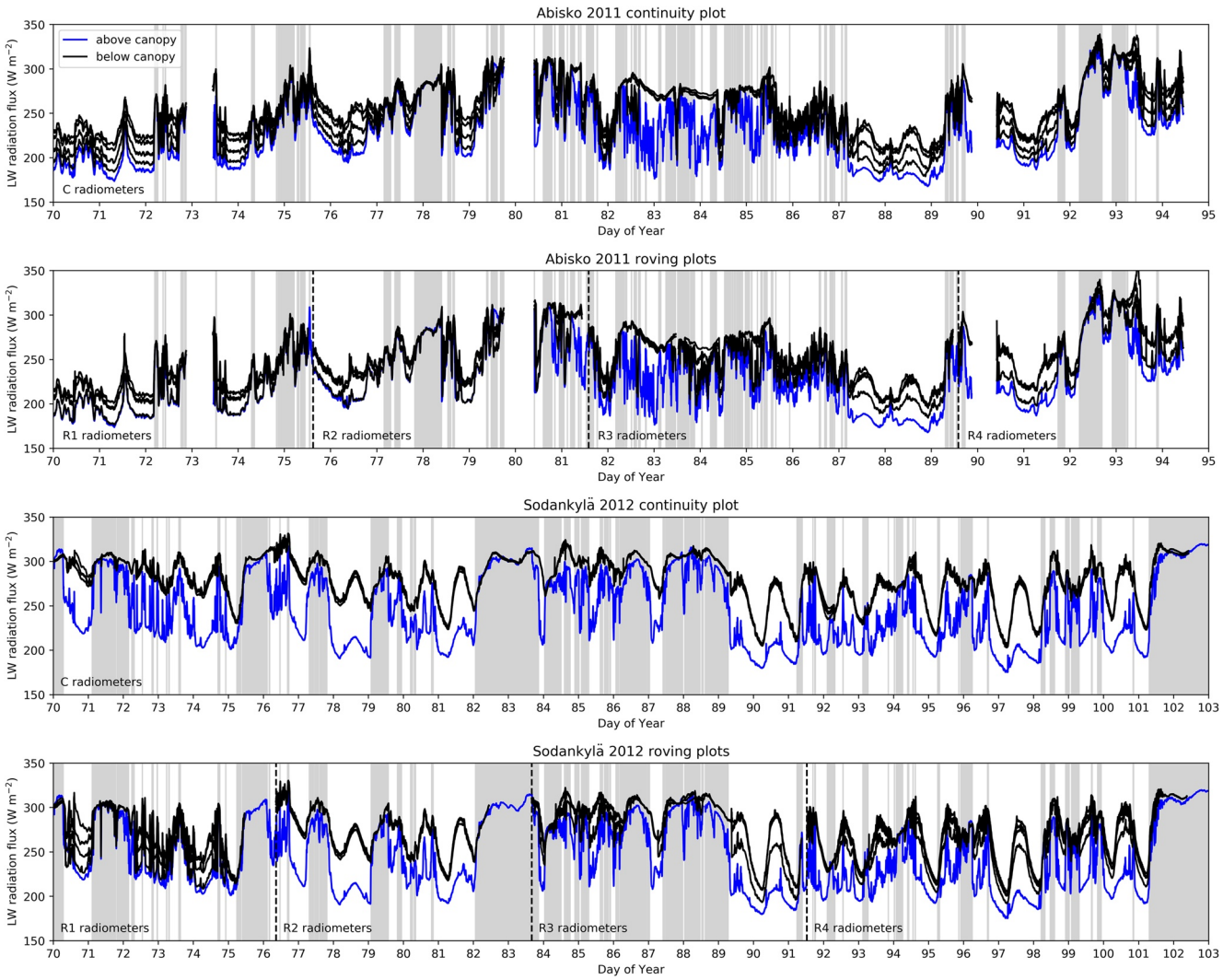

Figure A1. Above and below canopy incoming longwave radiation (black—four individual sub-canopy sensors, blue—above single canopy sensor), gray shading indicating when $\epsilon_a > 0.9$. Dashed lines in roving plots indicate transition of sensors between plots.

Appendix B

To put it in context, FSM2 represents canopy process with a similar level of complexity to the widely used Community Land Model; Lawrence et al., 2020). Sensible heat fluxes are parametrized as

$$H_s = \frac{\rho c_p}{r_s}(T_s - T_{ac}) \tag{B1}$$

from the ground surface at temperature T_s to the within-canopy air space at temperature T_{ac},

$$H_c = \frac{\rho c_p}{r_c}(T_c - T_{ac}) \tag{B2}$$

from the canopy at temperature T_c to the within-canopy air space, and

$$H = \frac{\rho c_p}{r_a}(T_{ac} - T_a) \tag{B3}$$

from the within-canopy air space to the above-canopy air at temperature T_a. Here, ρ and c_p are the density and heat capacity of air, and r_a, r_c, and r_s are aerodynamic resistances that depend on wind speed, canopy height and leaf area index. FSM2 has options to include or neglect an increase in r_a for stable atmospheric conditions ($T_{ac} < T_a$).

For this sensitivity study, the surface and canopy energy balances are simplified by assuming a dry and non-transpiring canopy (so no latent heat flux) at night (so no shortwave radiation) with low temperatures (so no snowmelt) and in steady state (so no heat storage terms). Balances between net longwave radiation and sensible heat fluxes are then

$$H_c = (1 - f_v)\left(LW_a - 2\sigma T_c^4 + \sigma T_s^4\right) \tag{B4}$$

for the canopy and

$$H_s = f_v LW_a + (1 - f_v)\sigma T_c^4 - \sigma T_s^4 \tag{B5}$$

for the surface. Together with the constraint $H = H_c + H_s$, Equations B4 and B5 can be solved iteratively to find T_{ac}, T_c and T_s.

Figure B1 shows within-canopy, canopy and surface temperatures relative to above-canopy air temperature as functions of wind speed for a stable nighttime case with $T_a = -3$°C and $LW_a = 271$ W m^{-2} ($\varepsilon_a = 0.9$). At very low wind speeds, the turbulent fluxes decay and the temperatures approach the apparent blackbody temperature of the sky (7°C lower than the above-canopy air temperature in this case). Temperatures decrease faster with decreasing wind speed if a stability adjustment is used. At higher wind speeds, the well-ventilated canopy and canopy air space temperatures approach the above-canopy air temperature but the ground remains colder.

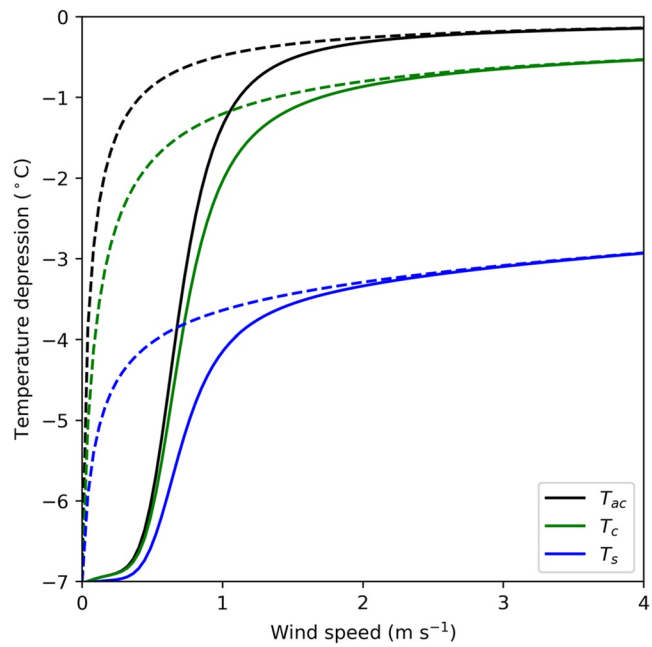

Figure B1. Within-canopy air space, canopy and ground surface temperatures relative to above-canopy air temperature as functions of wind speed. Solid lines were calculated with and dashed lines without adjustment for atmospheric stability.

Appendix C

The fraction of the sky obscured by a trunk of height h and radius r is

$$v_t = \frac{\sin^{-1}\left[(1 + d/r)^{-1}\right]}{\pi(1 + d/h)}, \tag{C1}$$

which decreases rapidly with distance d from the trunk. This corrects an error in equation A6 of Woo and Giesbrecht (2000).

Data Availability Statement

Abisko data (NERC et al., 2013a) and Sodankylä data (NERC et al., 2013b) used within this study are freely available from the Centre for Environmental Data Analysis.

Acknowledgments
The authors would like to acknowledge the staff at ANS, Sweden and FMI-ARC, Finland, for help and support during data collection. In particular, we are grateful to Timo Ryyppö of FMI-ARC for providing tower-mounted air temperature data at Sodankylä. Funding for this study was provided from the UK's Natural Environment Research Council (NERC) Grants NE/H008187/1 (to Essery), NE/H005013/1 (to Huntley and Baxter), NE/H005099/1 (to Rutter) and a Northumbria RDF Studentship (to Horton).

References

Broxton, P. D., Harpold, A. A., Biederman, J. A., Troch, P. A., Molotch, N. P., & Brooks, P. D. (2015). Quantifying the effects of vegetation structure on snow accumulation and ablation in mixed-conifer forests. *Ecohydrology*, *8*(6), 1073–1094. https://doi.org/10.1002/eco.1565

De Frenne, P., Lenoir, J., Luoto, M., Scheffers, B. R., Zellweger, F., Aalto, J., et al. (2021). Forest microclimates and climate change: Importance, drivers and future research agenda. *Global Change Biology*, *27*(11), 2279–2297. https://doi.org/10.1111/gcb.15569

Essery, R. (2015). A factorial snowpack model (FSM 1.0). *Geoscientific Model Development*, *8*(12), 3867–3876. https://doi.org/10.5194/gmd-8-3867-2015

Essery, R., Kontu, A., Lemmetyinen, J., Dumont, M., & Ménard, C. B. (2016). A 7-year dataset for driving and evaluating snow models at an Arctic site (Sodankylä, Finland). *Geoscientific Instrumentation, Methods and Data Systems*, *5*(1), 219–227. https://doi.org/10.5194/gi-5-219-2016

Essery, R., Pomeroy, J., Ellis, C., & Link, T. (2008). Modelling longwave radiation to snow beneath forest canopies using hemispherical photography or linear regression. *Hydrological Processes*, *22*(15), 2788–2800. https://doi.org/10.1002/hyp.6930

Foken, T. (2022). Decoupling between the atmosphere and the underlying surface during stable stratification. *Boundary-Layer Meteorology*, *187*(1–2), 117–140. https://doi.org/10.1007/s10546-022-00746-1

Gouttevin, I., Lehning, M., Jonas, T., Gustafsson, D., & Mölder, M. (2015). A two-layer canopy model with thermal inertia for an improved snowpack energy balance below needleleaf forest (model SNOWPACK, version 3.2.1, revision 741). *Geoscientific Model Development*, *8*(8), 2379–2398. https://doi.org/10.5194/gmd-8-2379-2015

Hancock, S., Essery, R., Reid, T., Carle, J., Baxter, R., Rutter, N., & Huntley, B. (2014). Characterising forest gap fraction with terrestrial lidar and photography: An examination of relative limitations. *Agricultural and Forest Meteorology*, *198–190*, 105–114. https://doi.org/10.1016/j.agrformet.2014.01.012

Hotovy, O., & Jenicek, M. (2020). The impact of changing subcanopy radiation on snowmelt in a disturbed coniferous forest. *Hydrological Processes*, *34*(26), 5298–5314. https://doi.org/10.1002/hyp.13936

Jonas, T., Webster, C., Mazzotti, G., & Malle, J. (2020). HPEval: A canopy shortwave radiation transmission model using high-resolution hemispherical images. *Agricultural and Forest Meteorology*, *284*, 107903. https://doi.org/10.1016/j.agrformet.2020.107903

Kangas, M., Rontu, L., Fortelius, C., Aurela, M., & Poikonen, A. (2016). Weather model verification using Sodankylä mast measurements. *Geoscientific Instrumentation, Methods and Data Systems*, *5*(1), 75–84. https://doi.org/10.5194/gi-5-75-2016

Lawler, R. L., & Link, T. E. (2011). Quantification of incoming all-wave radiation in discontinuous forest canopies with application to snowmelt prediction. *Hydrological Processes*, *25*(21), 3322–3331. https://doi.org/10.1002/hyp.8150

Lawrence, D., Fisher, R., Koven, C., Oleson, K., Swenson, S., Vertenstein, M., et al. (2020). Technical description of version 5.0 of the Community Land Model (CLM). https://www2.cesm.ucar.edu/models/cesm2/land/CLM50_Tech_Note.pdf

Link, T. E., & Marks, D. (1999). Point simulation of seasonal snow cover dynamics beneath boreal forest canopies. *Journal of Geophysical Research*, *104*(D22), 27841–27857. https://doi.org/10.1029/1998JD200121

Lundquist, J. D., Chickadel, C., Cristea, N., Currier, W. R., Henn, B., Keenan, E., & Dozier, J. (2018). Separating snow and forest temperatures with thermal infrared remote sensing. *Remote Sensing of Environment*, *209*, 764–779. https://doi.org/10.1016/j.rse.2018.03.001

Lundquist, J. D., Dickerson-Lange, S. E., Lutz, J. A., & Cristea, N. C. (2013). Lower forest density enhances snow retention in regions with warmer winters: A global framework developed from plot-scale observations and modeling. *Water Resources Research*, *49*(10), 6356–6370. https://doi.org/10.1002/wrcr.20504

Lundquist, J. D., Pepin, N., & Rochford, C. (2008). Automated algorithm for mapping regions of cold-air pooling in complex terrain. *Journal of Geophysical Research*, *113*(D22), D22107. https://doi.org/10.1029/2008JD009879

Malle, J., Rutter, N., Webster, C., Mazzotti, G., Wake, L., & Jonas, T. (2021). Effect of forest canopy structure on wintertime land surface albedo: Evaluating CLM5 simulations with in-situ measurements. *Journal of Geophysical Research: Atmospheres*, *126*(9), e2020JD034118. https://doi.org/10.1029/2020JD034118

Mazzotti, G., Essery, R., Moeser, C. D., & Jonas, T. (2020). Resolving small-scale forest snow patterns using an energy balance snow model with a one-layer canopy. *Water Resources Research*, *56*(1), e2019WR026129. https://doi.org/10.1029/2019WR026129

Mazzotti, G., Essery, R., Webster, C., Malle, J., & Jonas, T. (2020). Process-level evaluation of a hyper-resolution forest snow model using distributed multisensor observations. *Water Resources Research*, *56*(9), e2020WR027572. https://doi.org/10.1029/2020WR027572

Mazzotti, G., Malle, J., Barr, S., & Jonas, T. (2019). Spatially continuous characterization of forest canopy structure and subcanopy irradiance derived from handheld radiometer surveys. *Journal of Hydrometeorology*, *20*(7), 1417–1433. https://doi.org/10.1175/jhm-d-18-0158.1

Moeser, C. D., Broxton, P. D., Harpold, A., & Robertson, A. (2020). Estimating the effects of forest structure changes from wildfire on snow water resources under varying meteorological conditions. *Water Resources Research*, *56*(11), e2020WR027071. https://doi.org/10.1029/2020WR027071

Moeser, D., Roubinek, J., Schleppi, P., Morsdorf, F., & Jonas, T. (2014). Canopy closure, LAI and radiation transfer from airborne LiDAR synthetic images. *Agricultural and Forest Meteorology*, *197*, 158–168. https://doi.org/10.1016/j.agrformet.2014.06.008

Morsdorf, F., Kötz, B., Meier, E., Itten, K. I., & Allgöwer, B. (2006). Estimation of LAI and fractional cover from small footprint airborne laser scanning data based on gap fraction. *Remote Sensing of Environment*, *104*(1), 50–61. https://doi.org/10.1016/j.rse.2006.04.019

Musselman, K. N., Molotch, N. P., Margulis, S. A., Kirchnerd, P. B., & Bales, R. C. (2012). Influence of canopy structure and direct beam solar irradiance on snowmelt rates in a mixed conifer forest. *Agricultural and Forest Meteorology*, *161*, 46–56. https://doi.org/10.1016/j.agrformet.2012.03.011

Musselman, K. N., & Pomeroy, J. W. (2017). Estimation of needleleaf canopy and trunk temperatures and longwave contribution to melting snow. *Journal of Hydrometeorology*, *18*(2), 555–572. https://doi.org/10.1175/jhm-d-16-0111.1

NERC, Essery, R., Huntley, B., & Rutter, N. (2013a). Snow-vegetation-atmosphere interactions over heterogeneous landscapes project: Vegetation and meteorological observations at the Abisko site [dataset]. NCAS British Atmospheric Data Centre. Retrieved from http://catalogue.ceda.ac.uk/uuid/6947880b98d32e249a8638ebe768efd2 20 March 2023.

NERC, Essery, R., Huntley, B., & Rutter, N. (2013b). Snow-vegetation-atmosphere interactions over heterogeneous landscapes project: Vegetation and meteorological observations at the Sodankylä site [dataset]. NCAS British Atmospheric Data Centre. Retrieved from http://catalogue.ceda.ac.uk/uuid/9c8c86ed78ae4836a336d45cbb6a757c 20 March 2023.

Pomeroy, J., Marks, D., Link, T., Ellis, C., Hardy, J., Rowlands, A., & Granger, R. (2009). The impact of coniferous forest temperature on incoming longwave radiation to melting snow. *Hydrological Processes*, *23*(17), 2513–2525. https://doi.org/10.1002/hyp.7325

Reid, T. D., & Essery, R. L. H. (2013). New methods to quantify canopy structure of leafless boreal birch forest from hemispherical photographs. *Open Journal of Forestry*, *3*(2), 70–74. https://doi.org/10.4236/ojf.2013.32012

Reid, T. D., Essery, R. L. H., Rutter, N., & King, M. (2014). Data-driven modelling of shortwave radiation transfer to snow through boreal birch and conifer canopies. *Hydrological Processes*, *28*(6), 2987. https://doi.org/10.1002/hyp.9849

Rowlands, A., Pomeroy, J., Hardy, J., Marks, D., Elder, K., & Melloh, R. (2002). Small-scale spatial variability of radiant energy for snowmelt in a mid-latitude sub-alpine forest. *Proceedings from the 59th Eastern Snow Conference*, 109–117.

Rutter, N., Essery, R., Pomeroy, J., Altimir, N., Andreadis, K., Baker, I., et al. (2009). Evaluation of forest snow processes models (SnowMIP2). *Journal of Geophysical Research*, *114*(D6), D06111. https://doi.org/10.1029/2008jd011063

Schwartz, A., McGowan, H., & Callow, N. (2021). Snowpack thermal patterns in pre- and post-bushfire Snow Gum forests. *Journal of Hydrology*, *602*, 126789. https://doi.org/10.1016/j.jhydrol.2021.126789

Sicart, J. E., Pomeroy, J. W., Essery, R. L. H., & Bewley, D. (2006). Incoming longwave radiation to melting snow: Observations, sensitivity and estimation in northern environments. *Hydrological Processes*, *20*(17), 3697–3708. https://doi.org/10.1002/hyp.6383

Sicart, J. E., Pomeroy, J. W., Essery, R. L. H., Hardy, J., Link, T., & Marks, D. (2004). A sensitivity study of daytime net radiation during snowmelt to forest canopy and atmospheric conditions. *Journal of Hydrometeorology - Special Section*, *5*, 774–784. https://doi.org/10.1175/1525-7541(2004)005<0774:assodn>2.0.co;2

Thomas, G., & Rowntree, P. R. (1992). The boreal forests and climate. *Quarterly Journal of the Royal Meteorological Society*, *118*(505), 469–497. https://doi.org/10.1002/qj.49711850505

Todt, M., Rutter, N., Fletcher, C. G., & Wake, L. M. (2019). Simulated single-layer forest canopies delay Northern Hemisphere snowmelt. *The Cryosphere*, *13*(11), 3077–3091. https://doi.org/10.5194/tc-13-3077-2019

Todt, M., Rutter, N., Fletcher, C. G., Wake, L. M., Bartlett, P. A., Jonas, T., et al. (2018). Simulation of longwave enhancement in boreal and Montane forests. *Journal of Geophysical Research: Atmospheres*, *123*(24), 13731–13747. https://doi.org/10.1029/2018JD028719

Viterbo, P., & Betts, A. K. (1999). Impact on ECMWF forecasts of changes to the albedo of the boreal forests in the presence of snow. *Journal of Geophysical Research*, *104*(D22), 27803–27810. https://doi.org/10.1029/1998JD200076

Webster, C., Mazzotti, G., Essery, R., & Jonas, T. (2020). Enhancing airborne LiDAR data for improved forest structure representation in shortwave transmission models. *Remote Sensing of Environment*, *249*, 112017. https://doi.org/10.1016/j.rse.2020.112017

Webster, C., Rutter, N., & Jonas, T. (2017). Improving representation of canopy temperatures for modeling subcanopy incoming longwave radiation to the snow surface. *Journal of Geophysical Research: Atmospheres*, *122*(17), 9154–9172. https://doi.org/10.1002/2017JD026581

Webster, C., Rutter, N., Zahner, F., & Jonas, T. (2016). Modeling subcanopy incoming longwave radiation to seasonal snow using air and tree trunk temperatures. *Journal of Geophysical Research: Atmospheres*, *121*(3), 1220–1235. https://doi.org/10.1002/2015JD024099

Webster, C., Westoby, M., Rutter, N., & Jonas, T. (2018). Three-dimensional thermal characterization of forest canopies using UAV photogrammetry. *Remote Sensing of Environment*, *209*, 835–847. https://doi.org/10.1016/j.rse.2017.09.033

Woo, M., & Giesbrecht, M. A. (2000). Simulation of snowmelt in a subarctic spruce woodland: 1. Tree model. *Water Resources Research*, *36*(8), 2275–2285. https://doi.org/10.1029/2000WR900094